Functional correlates of immediate early gene expression in mouse visual cortex

David Mahringer[1,2], Pawel Zmarz[1,2,3], Hiroyuki Okuno[4], Haruhiko Bito[5] & Georg B. Keller[1,2,6]

[1] *Friedrich Miescher Institute for Biomedical Research, Basel, Switzerland.*
[2] *Faculty of Natural Sciences, University of Basel, Basel, Switzerland.*
[3] *Current address: Department of Organismic and Evolutionary Biology and Center for Brain Science, Harvard University, Cambridge, MA 02138, USA.*
[4] *Department of Biochemistry and Molecular Biology, Kagoshima University Graduate School of Medical and Dental Sciences, Kagoshima, Kagoshima 890-8544, Japan.*
[5] *Department of Neurochemistry, Graduate School of Medicine, The University of Tokyo, Hongo 7-3-1, Bunkyo-ku, Tokyo 113-0033, Japan.*
[6] Lead contact*: georg.keller@fmi.ch*

During visual development, response properties of layer 2/3 neurons in visual cortex are shaped by experience. Both visual and visuomotor experience are necessary to coordinate the integration of bottom-up visual input and top-down motor-related input. Whether visual and visuomotor experience engage different plasticity mechanisms, possibly associated with the two separate input pathways, is still unclear. To begin addressing this, we measured the expression level of three different immediate early genes (IEG) (*c-fos*, *egr1* or *Arc*) and neuronal activity in layer 2/3 neurons of visual cortex before and after a mouse's first visual exposure in life, and subsequent visuomotor learning. We found that expression levels of all three IEGs correlated positively with neuronal activity, but that first visual and first visuomotor exposure resulted in differential changes in IEG expression patterns. In addition, IEG expression levels differed depending on whether neurons exhibited primarily visually driven or motor-related activity. Neurons with strong motor-related activity preferentially expressed EGR1, while neurons that developed strong visually driven activity preferentially expressed Arc. Our findings are consistent with the interpretation that bottom-up visual input and top-down motor-related input are associated with different IEG expression patterns and hence possibly also with different plasticity pathways.

**** Dear reader, please note this manuscript is formatted in a standard submission format. ****

INTRODUCTION

During first visuomotor exposure in life, experience with coupling between movement and visual feedback is thought to coordination inputs onto layer 2/3 neurons in primary visual cortex (V1) such that

individual neurons receive balanced and opposing top-down motor-related and bottom-up visual input (Attinger et al., 2017; Jordan and Keller, 2020; Leinweber et al., 2017). While visual input without visuomotor coupling is sufficient to establish normal visual responses in layer 2/3 neurons, the emergence of visuomotor mismatch responses is contingent on experience with visuomotor coupling (Attinger et al., 2017) and requires on normal NMDA receptor dependent plasticity in the local V1 circuit (Widmer and Keller, 2021). How top-down and bottom-up inputs are coordinated during visual and visuomotor experience and whether plasticity mechanisms in the bottom-up visual driven pathway are the same as those engaged in the top-down motor-related input is still unclear. Here we set out to test for differences in plasticity mechanisms related to first exposure to visual input and first exposure to normal visuomotor coupling using concurrent measurement of neuronal activity and the expression levels of different immediate early gene (IEG) products as markers of plasticity in layer 2/3 of mouse visual cortex.

IEG products play a critical role in synaptic and neuronal plasticity during learning (Chowdhury et al., 2006; Fleischmann et al., 2003; Gandolfi et al., 2017; Jones et al., 2001; Messaoudi et al., 2007; Rial Verde et al., 2006; Shepherd and Bear, 2011; Shepherd et al., 2006; Tzingounis and Nicoll, 2006; Vazdarjanova et al., 2006; Veyrac et al., 2014; Waung et al., 2008) and are necessary for long-term memory consolidation (Bozon et al., 2003; Fleischmann et al., 2003; Guzowski, 2002; Guzowski and McGaugh, 1997; Guzowski et al., 2000; Jones et al., 2001; Ploski et al., 2008; Yasoshima et al., 2006). Ever since the discovery that the expression of the transcription factor c-Fos can be induced by electrical or chemical stimulation in neurons (Greenberg and Ziff, 1984), the expression of IEGs has been used as a marker for neuronal activity (Bullitt, 1990; Guzowski et al., 1999; Jarvis et al., 2000; Knapska and Kaczmarek, 2004; Minatohara et al., 2015; Morgan et al., 1987; Ramírez-Amaya et al., 2005; Reijmers et al., 2007; Wang et al., 2021). Based on the discovery that certain forms of episodic memory can be reactivated by artificially activating an ensemble of neurons characterized by high IEG expression levels during memory acquisition (Denny et al., 2014; Garner et al., 2012; Liu et al., 2012; Ramirez et al., 2013), it has been speculated that IEG expression is related not simply to neuronal activity *per se*, but to the induction of activity-dependent plasticity (Holtmaat and Caroni, 2016; Josselyn et al., 2015; Kaplan et al., 1996). Assuming IEG expression is indeed related to the induction of neuronal plasticity, it is conceivable that different IEGs are preferentially involved in plasticity of different synapse types or input pathways. c-Fos and EGR1 expression levels in visual cortex, for example, are differentially regulated by visual experience and exhibit a differential dependence on neuromodulatory input

63 (Yamada et al., 1999). Consistent with a pathway-specific role of Arc and EGR1 in visual cortex, it has
64 been shown that Arc is necessary for different forms of plasticity of bottom-up visual input, including
65 ocular dominance plasticity (Gao et al., 2010; Jenks et al., 2017; McCurry et al., 2010; Wang et al., 2006),
66 while a knockout of *egr1* has been shown to leave ocular dominance plasticity unaffected (Mataga et al.,
67 2001). It is still unclear however, whether IEG expression is differentially regulated by changes in
68 bottom-up and top-down input and if there is preferential expression of different IEGs in neurons that
69 are predominantly excited by top-down motor-related input as compared to neurons that are
70 predominantly excited by bottom-up visual input.

71 **RESULTS**

72 To measure both IEG expression levels and neuronal activity chronically, we used a combination of
73 transgenic mice that express GFP under the control of an IEG promoter and viral delivery of a red variant
74 of a genetically encoded calcium indicator. We did this for three different IEGs (*c-fos*, *egr1*, and *Arc*), in
75 three groups of mice separately. EGFP-Arc and c-Fos-GFP mice are transgenic mice that express a fusion
76 protein of Arc or c-Fos, and GFP downstream of either an *Arc* or a *c-fos* promoter, respectively (Barth et
77 al., 2004; Okuno et al., 2012), while the EGR1-GFP mouse expresses GFP under an *egr1* promotor (Xie et
78 al., 2014). Although there are a number of caveats to using GFP levels in these mouse lines as a proxy for
79 IEG expression levels (see discussion), there is a strong overlap between post-mortem antibody staining
80 for the respective IEG and GFP expression in all three mouse lines (Barth et al., 2004; Okuno et al., 2012;
81 Xie et al., 2014; Yassin et al., 2010). Throughout the manuscript, we will use IEG expression to mean GFP
82 expression levels in these mice. To measure calcium activity, we used an AAV2/1-Ef1a-jRGECO1a viral
83 vector to express the genetically encoded red calcium indicator jRGECO1a (Dana et al., 2016). This
84 biased our recordings to excitatory neurons, as in the first few weeks after the injection, the Ef1a
85 promoter restricts expression mainly to excitatory neurons (Attinger et al., 2017).

86 To quantify the correlation between neuronal activity and IEG expression in layer 2/3 of visual cortex in
87 adult mice, we first used a paradigm of dark adaptation and subsequent brief visual exposure (**Figure**
88 **1A**). We did this in three groups of adult mice separately (4 EGFP-Arc mice, 4 c-Fos-GFP mice, and 4
89 EGR1-GFP mice, between 100 and 291 days old). We dark-adapted all three groups of mice for 24 hours
90 and subsequently head-fixed them, while still in complete darkness, under a two-photon microscope on
91 a spherical treadmill (**Figure 1A**). We then measured calcium activity and IEG levels every 15 minutes for
92 six hours (**Figures 1B-1D**; see Methods). Between the first and second measurement, mice were exposed
93 to visual input for 15 minutes. This paradigm, which is a combination of light exposure and exposure of

94 the mouse to head-fixation, resulted in transient and modest increases in Arc and EGR1 expression
95 levels, and a decrease in c-Fos expression levels (**Figure S1A**). Given that mean neuronal activity levels in
96 V1 are rapidly stabilized across light-dark transitions (Hengen et al., 2016), and only a prolonged dark
97 adaption (of 60 hours) results in a substantial increase of neuronal activity upon light exposure (Torrado
98 Pacheco et al., 2019), the absence of a strong IEG response is perhaps not surprising.

99 To quantify the relationship between neuronal activity and IEG expression levels more directly, we then
100 computed the correlation between average neuronal activity and IEG expression levels for each neuron
101 as a function of time between neuronal activity measurement and IEG expression measurement (**Figures**
102 **1E-1G**). Correlation peaked at a time lag of approximately 3.5 h ± 0.5 h (mean ± SEM) between neuronal
103 activity measurement and IEG measurement for Arc and c-Fos, and was positive but relatively stable in a
104 window from -2 hours to +3 hours for EGR1 consistent with previous results (Wang et al., 2021)(Arc:
105 1382 neurons, c-Fos: 1070 neurons, EGR1: 1319 neurons; **Figures 1E-1G**). At peak, the correlation
106 between neuronal activity and IEG expression was highest for c-Fos, intermediate for Arc, and lowest for
107 EGR1 (**Figures 1H-1J**; correlation coefficients for c-Fos: 0.39 ± 0.07, Arc: 0.26 ± 0.05, EGR1: 0.21 ± 0.03,
108 mean ± SEM; comparisons between c-Fos vs. Arc: $p < 3 \times 10^{-4}$, Arc vs. EGR1: $p = 0.0188$, c-Fos vs. EGR1: p
109 $< 10^{-8}$; 4 mice per group, t-test with bootstrapping, see Methods). The positive correlation and the time
110 lag of the correlation peak would be consistent with the idea that neuronal activity induces IEG
111 expression, but the fact that correlations with mean activity were relatively weak could mean that it is
112 specific patterns or types of activity that induce IEG expression. It is often assumed that IEG expression
113 is also a correlate of neuronal plasticity (Holtmaat and Caroni, 2016; Josselyn et al., 2015; Kaplan et al.,
114 1996). Given that certain forms of neuronal plasticity are associated with bursts of activity, we first
115 tested whether maximum activity was a better predictor of IEG expression levels than mean activity.
116 Indeed, we found that the correlation with maximum neuronal activity was higher than the correlation
117 with mean activity for all three IEGs, but only significantly so for Arc and EGR1 (**Figure S1B**). Thus, the
118 fact that we could detect a positive, albeit weak, relationship between neuronal calcium activity and IEG
119 expression, would suggest that the method of using transgenic mice that drive GFP under an IEG
120 promoter has sufficient resolution to detect physiologically relevant changes in IEG levels.

121 We thus proceeded to apply the same methods of measuring IEG dynamics and neuronal calcium
122 activity during a mouse's first exposure to visual input and subsequent first exposure to normal
123 visuomotor coupling. To investigate whether first visual and first visuomotor exposure results in a
124 differential expression of immediate early genes, we used a virtual reality system to experimentally

separate first visual exposure and first exposure to normal visuomotor coupling. To do this, we reared mice in complete darkness and quantified both IEG expression levels and neuronal activity before and after mice were exposed to visual input for the first time in life as well as during a subsequent phase of visuomotor learning. Under normal conditions, first visual exposure is coincident with exposure to normal visuomotor coupling. At eye opening, mice are capable of moving eyes, head, and body and thus immediately experience self-generated visual feedback. To experimentally separate the moment of first visual exposure from first exposure to normal visuomotor coupling, we recorded neuronal activity and IEG expression as mice transitioned through three different experimental conditions. Prior to experiments, three groups of mice were reared in complete darkness until postnatal day 40 (7 EGFP-Arc mice, 5 c-Fos-GFP mice, and 4 EGR1-GFP mice). We then imaged neuronal activity and IEG expression levels every 12 hours for a total of 6 days. During all two-photon imaging experiments, mice were head-fixed on a spherical treadmill. During the first four recording sessions, mice were kept on the setup in darkness to measure locomotion-related and non-visual activity and remained dark housed in between recording sessions (condition 1). At the beginning of the 5th recording session, mice were then exposed to visual input for the first time in their life. In the subsequent four recording sessions, mice were exposed to different virtual environments but remained housed in darkness in the time between the recording sessions (condition 2). In addition to recording activity in darkness, recording sessions in condition 2 also contained 8 min of closed-loop feedback during which visual flow on the walls of a virtual corridor was coupled to the mouse's locomotion on the spherical treadmill. During closed-loop feedback, we added brief halts of visual flow to probe for visuomotor mismatch responses (Keller et al., 2012). This was followed by a phase of open-loop feedback during which the visual flow generated by the mouse during the closed-loop feedback was replayed independently of the locomotion of the mouse. Lastly, we presented a series of drifting gratings to the mouse to quantify visual responses (see Methods). Following recording session 8, mice were introduced to a normal 12 h light / 12 h dark cycle. At this time, mice first experienced normal visuomotor coupling in their home cage. We continued recording for an additional four sessions (condition 3) with the same series of closed-loop, open-loop and grating stimulation phases as in condition 2 (**Figure 2A**). Recording sessions lasted on average 12 min ± 0.5 min (mean ± SEM) in condition 1, and 83 min ± 1 min (mean ± SEM) in conditions 2 and 3 (**Figure S2**). Note, to probe for different visuomotor mismatch responses, condition 2 already contains a short period of head-fixed, closed-loop feedback. Given the short duration and the fact that coupling here is only in a small subspace (forward locomotion coupled to backward visual flow and normal coupling for eye movements) of the total space of visuomotor coupling, we would expect the exposure

157 to normal visuomotor coupling in condition 3 to have a stronger influence on visuomotor integration.
158 The aim of this paradigm was to experimentally separate the first visual exposure at the beginning of
159 condition 2, from the first exposure to normal visuomotor coupling at the beginning of condition 3.

160 It has been shown that visual input can drive the expression of different IEGs in a subset of neurons in
161 visual cortex (Kaminska et al., 1996; Kawashima et al., 2013; Rosen et al., 1992; Tagawa et al., 2005;
162 Wang et al., 2006). Based on this it is sometimes assumed that neuronal activity in visual cortex is higher
163 with visual input than it is in darkness. Differences in neuronal activity between light and dark, however,
164 are small and predominantly transient (Fiser et al., 2004; Hengen et al., 2016; Torrado Pacheco et al.,
165 2019). To test whether in our paradigm first visual exposure or first exposure to normal visuomotor
166 coupling results in an increase of average neuronal activity in visual cortex, we quantified average
167 neuronal activity in each recording session (in condition 1 this only included recordings in darkness,
168 while in conditions 2 and 3 this included recordings in darkness, closed and open-loop feedback, as well
169 as drifting gratings). Consistent with a strong motor-related drive in visual cortex (Keller et al., 2012;
170 Saleem et al., 2013) and rapid homeostatic restoration of average activity following removal of visual
171 input (Keck et al., 2013), we found no evidence of an increase of average neuronal activity at the onset
172 of either condition 2 (first visual exposure) or condition 3 (first exposure to normal visuomotor coupling)
173 (**Figure 2B**). To the contrary, following the first visual exposure, there was a trend for decreasing activity
174 levels ($p = 0.0293$, $R^2 = 0.371$, linear trend analysis, see Methods). We next quantified average
175 expression of Arc, c-Fos and EGR1 over the same time course. Consistent with the absence of a change
176 in average activity levels, we found no significant changes in the expression levels of any of the three
177 IEGs following the first visual exposure at the beginning of condition 2 (**Figure 2C**). Note, we cannot
178 exclude that there is a transient increase in IEG expression between 1 h and 12 h following first visual
179 exposure, as we only recorded for 1 hour every 12 hours. We did however find that the first exposure to
180 normal visuomotor coupling at the beginning of condition 3, resulted in an increase in the expression of
181 Arc and a decrease in the expression of EGR1 in the absence of a measurable change in average
182 neuronal activity levels (**Figure 2C**). To test for changes in the pattern of IEG expression, we quantified
183 the similarity of IEG expression patterns by computing the correlation of IEG expression vectors
184 between imaging time points (see Methods). We found that the pattern of Arc expression changed both
185 with the first visual exposure (onset of condition 2) and the first exposure to normal visuomotor
186 coupling (onset of condition 3) (**Figure 2D**). The pattern of c-Fos expression exhibited no detectable
187 discontinuous changes (**Figure 2E**), while the pattern of EGR1 expression exhibited a marked transition
188 with the first exposure to normal visuomotor coupling (onset of condition 3) (**Figure 2F**). This suggests

189 that the expression patterns of IEGs are differentially and dynamically regulated by visuomotor
190 experience, also in absence of population mean expression level changes.

191 Neurons in layer 2/3 of primary visual cortex are driven differentially by visual and motor-related inputs
192 (Attinger et al., 2017; Keller et al., 2012; Leinweber et al., 2017). Given that the expression patterns of
193 the three IEGs are differentially altered by first visual exposure and first exposure to normal visuomotor
194 coupling, we speculated that the different IEGs could be preferentially expressed in different functional
195 types of excitatory neurons in layer 2/3. Neurons that are more strongly visually driven, likely by
196 bottom-up visual input, could have a different IEG expression profile than neurons that are more
197 strongly driven by top-down motor-related signals (Leinweber et al., 2017; Makino and Komiyama,
198 2015). To test this, we quantified the functional properties of the neurons with the highest IEG
199 expression levels immediately after the first exposure to normal visuomotor coupling where we
200 observed the largest mean IEG expression level changes (**Figure 2C**). We selected the 10 % of neurons
201 with the highest Arc, c-Fos and EGR1 expression, respectively, at the beginning of condition 3 (Arc: 197
202 neurons, c-Fos: 189 neurons, EGR1: 121 neurons) and tested whether these neurons were more strongly
203 driven by visual or motor-related input. As a measure of the strength of the motor-related input, we
204 used the magnitude of the neuronal response during running onsets in darkness. We found that neurons
205 with high EGR1 expression levels developed higher motor-related responses than the rest of the
206 population in both condition 2 and condition 3. Conversely, neurons with high Arc expression levels
207 developed motor-related responses that are lower than the rest of the population following exposure to
208 normal visuomotor coupling. Responses in neurons with high c-Fos expression levels were not different
209 from responses in the rest of the population (**Figure 3A**). To quantify the strength of visual input we
210 used the magnitude of the neuronal response to drifting grating stimuli. Consistent with the fact that
211 Arc expression can be selectively induced by visual stimuli in a stimulus-specific manner (Kawashima et
212 al., 2013), we found that neurons with high Arc expression levels developed responses to drifting grating
213 stimuli that were stronger than the rest of the population after exposure to normal visuomotor
214 coupling. The drifting grating responses of neurons with high EGR1 or c-Fos expression levels were not
215 different from the mean population response (**Figure 3B**). Thus, neurons with high levels of EGR1
216 expression after first exposure to normal visuomotor coupling were more strongly driven by motor-
217 related input, while those with high levels of Arc expression were more strongly driven by visual input.

218 One of the signals that has been speculated to be computed in mouse primary visual cortex that
219 combines visual and motor-related input is visuomotor mismatch (Attinger et al., 2017; Keller et al.,

2012; Zmarz and Keller, 2016). Neurons that respond to mismatch, or negative prediction errors, are thought to receive excitatory motor-related input and inhibitory visual input (Attinger et al., 2017; Keller and Mrsic-Flogel, 2018). We speculated that given the increased motor-related activity in neurons that express high levels of EGR1, neuronal activity in these neurons should correlate positively with running, while activity in neurons that express high levels of Arc should correlate positively with visual flow. To quantify this, we computed the correlation of neuronal activity with either running or visual flow during the open-loop phases in conditions 2 and 3 for the three groups of neurons with high IEG expression levels. We found that the activity of neurons expressing high levels of EGR1 correlated most strongly with running, while the activity of neurons with high levels of Arc expression correlated positively with visual flow (**Figure 4A**). Consistent with this we found that visuomotor mismatch responses were larger in neurons with high EGR1 expression than in the rest of the population, while they were lower in neurons with high Arc expression than in the rest of the population (**Figure 4B**). This indicates that, at the onset of normal visuomotor coupling, EGR1 is preferentially expressed in mismatch neurons or, more generally, in neurons that are driven by excitatory top-down input, while Arc is preferentially expressed in neurons that are driven by bottom-up visual input.

DISCUSSION

It is well established that both neuronal activity and plasticity are linked to the expression of immediate early genes (Dudek, 2008; Mahringer et al., 2019; Minatohara et al., 2015; Wang et al., 2021; Yap and Greenberg, 2018). Comparably little, however, is known about how specific functional characteristics of neurons relate to the expression of immediate early genes. Here we investigated the relationship between the expression of three IEGs (Arc, c-Fos, and EGR1) and functional responses in excitatory layer 2/3 neurons of mouse visual cortex. We found that during visuomotor learning following a mouse's first visual exposure in life, Arc was preferentially expressed in neurons that are driven by excitatory bottom-up visual input, while EGR1 was preferentially expressed in neurons that are driven by motor-related input. In addition, we found that neurons expressing high levels of EGR1 exhibit visuomotor mismatch responses higher than the rest of the population, while neurons expressing high levels of Arc exhibit visuomotor mismatch responses weaker than the rest of the population.

Such a relationship between a neuron's IEG expression profile and its functional properties could be explained by differences in the contribution of different IEGs to different types of input synapses. Arc, c-Fos, and EGR1 all have unique cellular functions, and it is conceivable that they make different contributions to different synapse types. Genes for a subset of $GABA_A$ receptor subunits, for example,

251 are transcriptional targets of EGR1 (Mo et al., 2015). If the postsynaptic subunit composition of the
252 GABA receptor is correlated with the presynaptic inhibitory cell type, EGR1 expression could
253 preferentially upregulate specific inhibitory input pathways. Similar input pathway-specific roles have
254 been described for other IEGs. Neuronal activity-regulated pentraxin (NARP) is secreted by pyramidal
255 neurons and exclusively accumulates at parvalbumin-positive inhibitory neurons where it regulates
256 excitatory synapses onto these cells (Chang et al., 2010; Gu et al., 2013). The activity-dependent
257 transcription factor NPAS4 has been found to restrict the number of synapses of mossy-fiber input
258 specifically onto CA3 pyramidal cells during learning (Weng et al., 2018).

259 Our data would be consistent with the interpretation that the IEG expression pattern of a given neuron
260 correlates with its pattern of synaptic inputs. Neurons that predominantly receive excitatory bottom-up
261 drive likely require a different distribution and type of input synapses compared to neurons that receive
262 mainly top-down excitatory drive. Layer 2/3 neurons that exhibit strong motor-related and mismatch
263 responses are thought to be driven by top-down excitatory inputs (Leinweber et al., 2017), which
264 predominantly target apical dendrites (Petreanu et al., 2009). Conversely, layer 2/3 neurons with strong
265 visual responses are thought to be driven by bottom-up visual inputs, which predominantly target basal
266 dendrites (Petreanu et al., 2009). We have speculated that mismatch neurons that receive motor-
267 related input also receive matched bottom-up inhibitory input from a specific subset of somatostatin
268 (SST)-positive interneurons (Attinger et al., 2017). Thus, EGR1 expression may be preferentially
269 increased in neurons that are driven by excitatory top-down input and SST mediated bottom-up
270 inhibition, while Arc expression may be preferentially increased in neurons that are driven by excitatory
271 bottom-up visual input. This may explain why a change to the visual input alone at first visual exposure
272 primarily resulted in a rearrangement of the Arc expression pattern (**Figure 2D**) but left the EGR1
273 expression pattern relatively unaffected (**Figure 2F**), while first exposure to normal visuomotor coupling
274 resulted in a rearrangement of the expression pattern of both Arc and EGR1.

275 When interpreting our results, it should be kept in mind that both the method we use to approximate
276 IEG expression levels and the method we use to approximate neuronal activity levels come with a series
277 of caveats. In the case of the transgenic mice used for the IEG expression measurements, two of these
278 express a fusion protein (Arc and c-Fos), where the IEG is likely overexpressed (Steward et al., 2017), and
279 it is possible that the decay kinetics of the fusion protein differ from those of the native protein. In the
280 case of the GFP driven by the *egr1* promoter, the GFP decay kinetics are likely different from the decay
281 kinetics of EGR1. However, these potential differences in decay kinetics and expression levels do not

282 completely mask the correlation between IEG expression levels and reporter proteins. In post-mortem
283 histological stainings the expression of GFP in these mouse lines overlaps well with the expression levels
284 of the IEGs (Barth et al., 2004; Okuno et al., 2012; Wang et al., 2021; Xie et al., 2014; Yassin et al., 2010).
285 Thus, reporter protein levels reflect a filtered version of IEG expression levels, and the two are likely
286 related by a monotonic function. Given that all our analyses rely only on relative expression levels
287 among populations of simultaneously recorded neurons or relative changes of expression levels in time,
288 the lack of a direct measurement of IEG expression levels should not change our conclusions. A second
289 caveat concerns the genetically encoded calcium indicator used to measure neuronal activity. Our
290 activity measures are biased towards bursts of neuronal activity, as single spikes are probably not always
291 detectable using calcium indicators *in vivo*. However, even though the transfer function from neuronal
292 activity to calcium signal is non-linear, it is also monotonic. Thus, we may be underestimating the
293 correlation between neuronal activity and IEG expression, but neither caveat would bias the results
294 towards finding specific correlations between different IEGs and functional cell types.

295 In summary, our results suggest that the expression of Arc and EGR1 in layer 2/3 neurons in mouse
296 visual cortex may be a correlate of the type of functional input the neuron receives. Such a preference
297 for expression in a functionally specific subset of neurons would be consistent with differential changes
298 in the ratio of the expression of different IEGs under conditions that result in identical mean levels of
299 neuronal activity (Bailey and Wade, 2003; Farina and Commins, 2016; Guzowski et al., 2006) that are
300 difficult to explain if IEG expression were simply driven by mean activity. In future experiments, it will be
301 important to establish a more detailed picture of how immediate early genes could orchestrate or
302 stabilize the pattern of functionally distinct input streams a neuron receives.

303 **FIGURES**

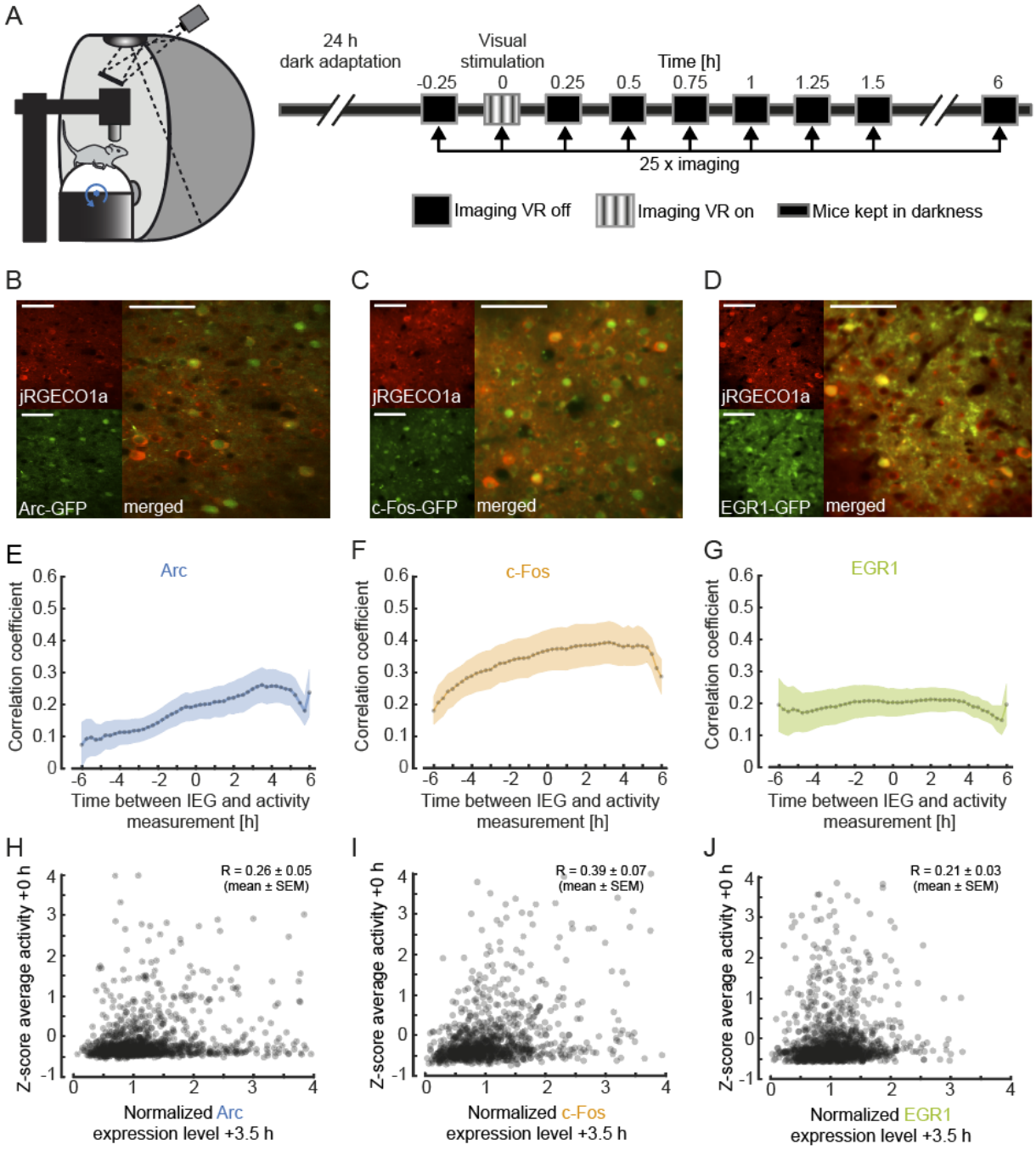

306 **Figure 1. Simultaneous imaging of neuronal activity and immediate early gene expression in visual**

307 **cortex.**

308 (**A**) Left: Schematic of the virtual reality setup used for imaging experiments. Right: Schematic of the
309 experimental timeline. Mice were dark-adapted for 24 hours. Neuronal activity and IEG expression levels
310 were recorded in 25 imaging sessions starting immediately before and continuing until 6 hours after
311 visual stimulation in intervals of 15 minutes.

312 (**B**) Example two-photon images of neurons in primary visual cortex labelled with jRGECO1a (red, top
313 left), Arc (green, bottom left), and the overlay (right). Scale bar is 50 μm.

314 (**C**) Same as in (**B**), but for c-Fos.

315 (**D**) Same as in (**B**), but for EGR1.

316 (**E**) Correlation of average activity and IEG expression level as a function of the time difference between
317 the two measurements. Dotted line indicates average correlation, shading indicates standard error of
318 the mean (SEM) across mice (n = 4).

319 (**F**) Same as in (**E**), but for c-Fos mice (n = 4).

320 (**G**) Same as in (**E**), but for EGR1 mice (n = 4).

321 (**H**) Scatter plot of Arc expression 3.5 hours after visual stimulation and average neuronal activity during
322 visual stimulation (1382 neurons in 4 mice, 83 neurons outside of plot range). Shown in the panel is the
323 average correlation coefficient across mice (mean ± SEM, n= 4).

324 (**I**) Same as in (**H**), but for c-Fos (1070 neurons in 4 mice, 28 neurons outside of plot range).

325 (**J**) Same as (**H**), but for EGR1 (1319 neurons in 4 mice, 18 neurons outside of plot range).

326

327

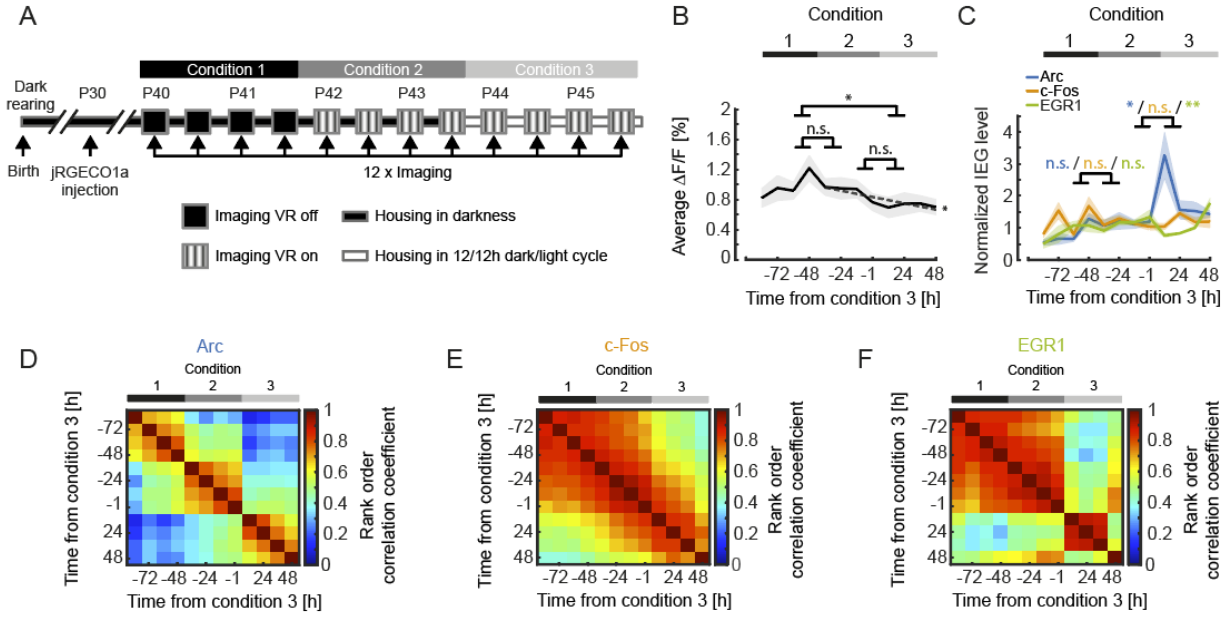

Figure 2. IEG expression dynamics during visuomotor learning.

(**A**) Schematic of the experimental timeline. Mice were born and reared in complete darkness. jRGECO1a was injected 10 to 12 days prior to the start of imaging experiments. We then imaged calcium activity and IEG expression levels every 12 h over the course of 6 days both before and after first visual exposure and first exposure to normal visuomotor coupling. On the first two days (condition 1) activity in visual cortex was recorded in complete darkness while mice were head-fixed and free to run on a spherical treadmill. On the third day of recording mice were exposed to visual feedback (first visual exposure) in a virtual reality environment. Outside of the recording sessions mice were still housed in complete darkness (condition 2). Starting on day 5, mice were subjected to a 12 h / 12 h light/dark cycle (condition 3).

(**B**) Average calcium activity during all conditions (condition 1 vs. 2: $p = 0.2183$, condition 2 vs. 3: $p = 0.527$, condition 1 vs. 3: $p = 0.0123$, 5067 neurons, paired t-test). Shading is SEM over mice. Dashed line indicates linear fit to the data of conditions 2 and 3. The linear fit to the data from conditions 2 and 3 exhibited a significant negative slope ($p = 0.0293$, $R^2 = 0.371$, linear trend analysis, see Methods).

(**C**) Normalized mean IEG expression levels during all conditions. Expression level of Arc (blue, 1969 neurons in 7 mice) significantly increased after first exposure to visuomotor coupling, decreased for EGR1 (green, 1213 neurons in 4 mice) and remained unchanged for c-Fos (orange, 1885 neurons in 5 mice). Change in IEG expression level between conditions 1 and 2 for Arc: 0.1764 ± 0.1556, $p = 0.2775$; c-Fos: -0.0536 ± 0.1877, $p = 0.7816$; EGR1: -0.0371 ± 0.1246, $p = 0.7745$ (mean ± SEM, paired t-test). Change in IEG expression level between conditions 2 and 3 for Arc: 1.2628 ± 0.5012, $p = 0.0256$; c-Fos: 0.01612 ± 0.1372, $p = 0.2702$; EGR1: -0.4568 ± 0.1130, $p = 0.0049$ (mean ± SEM, t-test). Shading indicates SEM over mice.

(**D**) Average rank order correlation coefficients for Arc expression during visuomotor learning (7 mice). The expression pattern changes both at the onset of conditions 2 and 3.

(**E**) Same as in (**D**), but for c-Fos (5 mice). The expression pattern exhibits no apparent transitions.

(**F**) Same as in (**D**), but for EGR1 (4 mice). The expression pattern changes at the onset of condition 3.

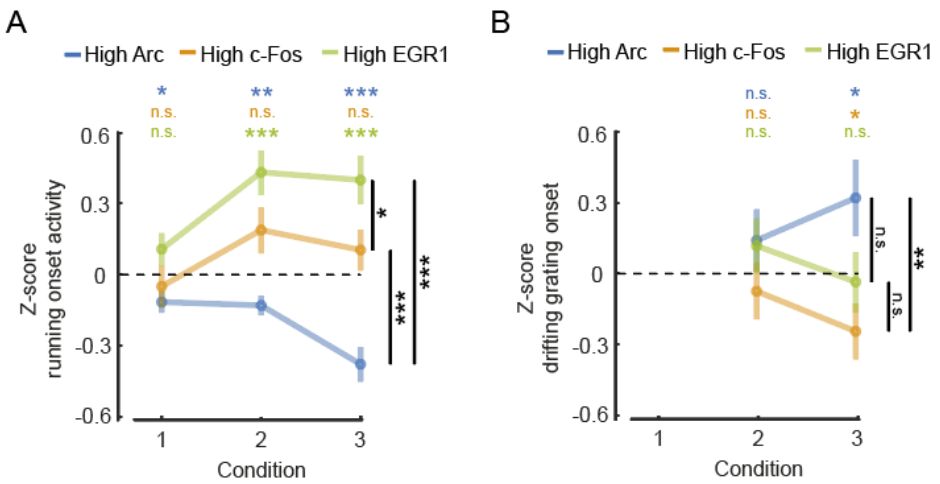

Figure 3. Differential relationship between IEG expression and motor-related and visual responses.

(**A**) Average running onset response during darkness for the top 10 % IEG expressing neurons (Arc: 197 neurons, c-Fos: 189 neurons, EGR1: 121 neurons). Neuronal responses were pooled from all experimental sessions for each condition, subtracted by the mean and normalized by the standard deviation of the response of all neurons (Z-score). Error bars are SEM over neurons. Statistics above the plot indicate comparisons against 0, statistics to the right are between-group comparisons. n.s.: $p > 0.05$, *: $p < 0.05$, **: $p < 0.01$, *** $p < 0.001$, t-test.

(**B**) Average grating onset response for the top 10 % IEG expressing neurons (Arc: n = 197, c-Fos: n = 189, EGR1: n = 121). Neuronal responses were pooled from all experimental sessions for conditions 2 and 3, subtracted by the mean and normalized by standard deviation of the response of all neurons (Z-score). Error bars are SEM over neurons. Statistics above the plot indicate comparisons against 0, statistics to the right are between-group comparisons. n.s.: $p > 0.05$, *: $p < 0.05$, **: $p < 0.01$, *** $p < 0.001$, t-test.

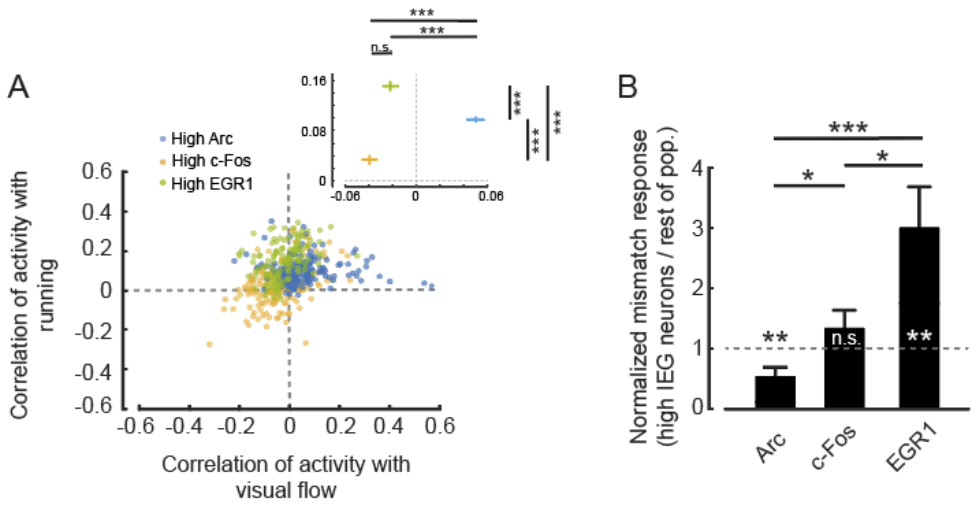

373 **Figure 4. Functional cell type specific expression of IEGs in visual cortex.**

374 (**A**) Correlation of neuronal activity with running and of neuronal activity with visual flow during open-
375 loop phases of conditions 2 and 3 for the top 10 % IEG expressing neurons (Arc: 197 neurons, c-Fos: 189
376 neurons, EGR1: 121 neurons). Inset: Average correlation coefficient for the three groups of high IEG
377 expressing neurons. High Arc expressing neurons had the highest correlation with visual flow (Arc vs. c-
378 Fos: $p < 10^{-10}$, Arc vs. EGR1: $p < 10^{-9}$, c-Fos vs. EGR1: $p = 0.0791$, t-test), while high EGR1 expressing
379 neurons had the highest correlation with running (Arc vs. c-Fos: $p < 10^{-10}$, Arc vs. EGR1: $p < 10^{-8}$, c-Fos vs.
380 EGR1: $p < 10^{-10}$, t-test).

381 (**B**) Mismatch responses in condition 3 were significantly higher for the top 10 % EGR1 expressing
382 neurons and significantly lower for the top 10 % Arc expressing neurons than the rest of the respective
383 population (Arc: 197 neurons, c-Fos: 189 neurons, EGR1: 121 neurons). Arc: $p = 0.0461$, c-Fos: $p =$
384 0.2273, EGR1: $p = 0.0234$; Arc vs. c-Fos: $p = 0.0101$, c-Fos vs. EGR1: $p = 0.048$, Arc vs. EGR1: $p = 0.0057$, t-
385 test.

386

387

388 **Supplementary Figures**

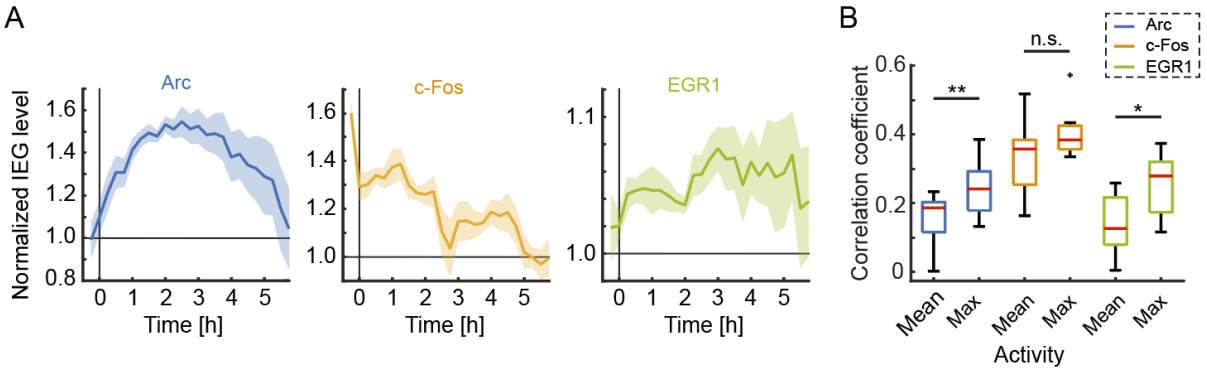

393 (**A**) Time course of normalized IEG expression levels following 24 h dark adaptation and 15 min visual
394 stimulation at time 0. Shading indicates SEM over neurons.

395 (**B**) Correlation coefficient of mean and maximum activity (average across or peak within a recording
396 session, respectively) with IEG expression 3.5 h after stimulation or recording onset (Arc: 11 mice, c-Fos:
397 9 mice, EGR1: 8 mice). Box whisker plot: red line indicates median, box marks 25th to 75th percentiles
398 and whiskers extended to the next most extreme datapoint within a range of 1.5 times the interquartile
399 distance (rank sum test, Arc: $p = 0.0086$, c-Fos: $p = 0.1359$, EGR1: $p = 0.0207$).

400

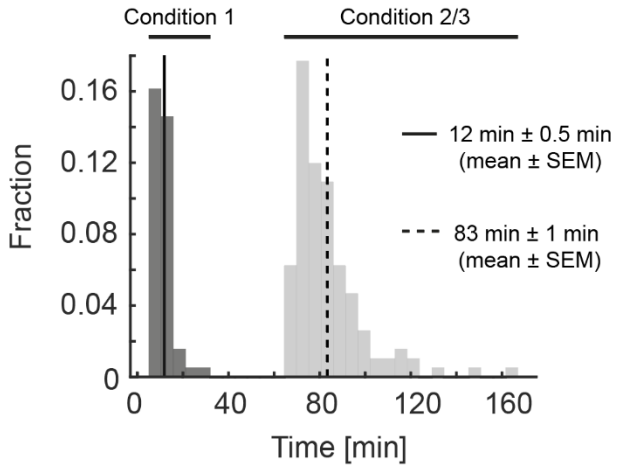

Figure S2. Duration of recording sessions. Related to Figure 2.

Histogram of the durations of the recording sessions. On average, one recording session lasted for approximately 12 min during condition 1 (solid line) and, due to the addition of closed-loop, open-loop, and grating stimulation phases, 83 min during conditions 2 and 3 (dashed line).

407 **METHODS**

408 **Animals and surgery.** All animal procedures were approved by and carried out in accordance with
409 guidelines of the Veterinary Department of the Canton Basel-Stadt, Switzerland. We used imaging data
410 from a total of 11 EGFP-Arc mice (Okuno et al., 2012), 9 c-Fos-GFP mice (Barth et al., 2004) and 8 EGR1-
411 GFP mice (Xie et al., 2014), aged 40 days at the start of visuomotor learning (**Figures 2 - 4**) or aged 100-
412 104 (Arc), 279-291 (c-Fos) or 120-124 (EGR1) days (**Figure 1**). Sample sizes were chosen according to the
413 standards in the field and no statistical methods were used to predetermine sample sizes. Mice were
414 group-housed in a dark cabinet and in a vivarium (light/dark cycle: 12 h / 12 h). Viral injections and
415 window implantation were performed as previously described (Dombeck et al., 2010; Leinweber et al.,
416 2014). Briefly, for sensorimotor learning experiments, mice (aged 29 d ± 1 d, mean ± SEM) were
417 anesthetized in darkness using a mix of fentanyl (0.05 mg/kg), medetomidine (0.5 mg/kg) and
418 midazolam (5 mg/kg), and additionally their eyes were covered with a thick, black cotton fabric during
419 all surgical procedures. A 3 mm to 5 mm craniotomy was made above visual cortex (2.5 mm lateral of
420 lambda (Paxinos and Franklin, 2013)) and AAV2/1-Ef1a-NES-jRGECO1a-WPRE ((Dana et al., 2016); titer:
421 between 7.2×10^{10} GC/ml and 6.8×10^{12} GC/ml) was injected into the target region. The craniotomy was
422 sealed with a fitting cover slip. A titanium head bar was attached to the skull and stabilized with dental
423 cement.

424 **Imaging and virtual reality.** Imaging commenced 10 – 12 (visuomotor learning experiments, **Figures 2 -**
425 **4**) or 12 – 29 (**Figure 1**) days following virus injection and was carried out using a custom-built two-
426 photon microscope. Illumination source was a Chameleon Vision laser (Coherent) tuned to a wavelength
427 of either 950 nm, 990 nm or 1030 nm. Imaging was performed using an 8 kHz resonance scanner
428 (Cambridge Technology) resulting in frame rates of 40 Hz at a resolution of 400 × 750 pixels. In addition,
429 we used a piezo actuator (Physik Instrumente) to move the objective (Nikon 16x, 0.8 NA) in steps of 15
430 µm between frames to acquire images at four different depths, thus reducing the effective frame rate to
431 10 Hz. The behavioral imaging setup was as previously described (Leinweber et al., 2014). After brief
432 isoflurane anesthesia mice were head-fixed in complete darkness and the setup was light-shielded
433 before every imaging session. Mice were free to run on an air-supported polystyrene ball, the motion of
434 which was restricted to the forward and backward directions by a pin. The ball's rotation was coupled to
435 linear displacement in the virtual environment that was projected onto a toroidal screen surrounding
436 the mouse. The screen covered a visual field of approximately 240 degrees horizontally and 100 degrees
437 vertically. All displayed elements of the tunnel or sinusoidal gratings were calibrated to be isoluminant.

438 **Experimental design.** For experiments shown in **Figure 1**, mice were dark-adapted for 24 h and 17 min ±
439 10 min (mean ± SEM, 12 mice) before head fixation under the microscope in darkness. Activity and
440 immediate early gene expression were recorded every 15 minutes for 6 hours. Except for the time of
441 visual stimulation with sinusoidal gratings moving in 8 different directions (a total of 80 presentation in
442 random order), mice were kept in complete darkness under the microscope for the duration of the
443 entire experiment. For visuomotor learning experiments (**Figures 2 - 4**) mice were born and reared in
444 complete darkness until P44 and then transferred to a vivarium with a 12 h /12 h light/dark cycle.
445 Experimental sessions started on P40 and occurred twice per day, spaced 12 h apart. In condition 1, all
446 imaging was done in complete darkness and experiments consisted of recording approximately 8 min of
447 neuronal activity during which mice were free to run on the spherical treadmill. IEG expression level
448 measurements were taken before and after each activity recording. In conditions 2 and 3, neuronal
449 activity measurements consisted of 7 recordings of approximately 8 minutes each. Each recording
450 session started with a recording in darkness, followed by a closed-loop recording. In the closed-loop
451 recording, the movement of the mouse in a linear virtual corridor (sinusoidal vertical grating) was
452 coupled to the locomotion of the mouse on the spherical treadmill. During the closed-loop session we
453 included brief (1 s) halts of visual flow to induce mismatch events (Attinger et al., 2017). The subsequent
454 two recordings were of the open-loop type and consisted of a playback of the visual flow the mouse had
455 generated during the preceding closed-loop recording. Subsequently, mice were exposed to a second
456 recording in darkness, followed by a visual stimulation recording. During the visual stimulation
457 sinusoidal moving grating stimuli (2 second standing grating, 3 second drifting grating, 8 different
458 orientations, 10 presentations of each orientation, in a randomized order) were presented. Finally, mice
459 were exposed to a third recording in darkness. In early phases of the experiment mice were encouraged
460 to run by applying occasional mild air puffs to the neck.

461 **Data analysis.** Imaging data were full-frame registered using a custom-written software (Leinweber et
462 al., 2014). Neurons were selected manually based on their mean fluorescence or maximum projection in
463 the red channel (jRGECO1a). This biased our selection towards active neurons. Fluorescence traces were
464 calculated as the mean pixel value in each region of interest per frame, and were then median-
465 normalized to calculate ΔF/F. ΔF/F traces were filtered as previously described (Dombeck et al., 2007).
466 GFP intensities were calculated as the mean pixel value in each region of interest (ROI) for mean
467 fluorescence projections. To compensate for expression level differences between different IEG mouse
468 lines as well as for image quality differences between different mice we normalized the GFP level

469 measurements as follows: For each mouse, all ROI measurements were subtracted by the minimum
470 calculated over all ROIs and timepoints, and normalized by the median over all ROIs and timepoints.

471 $$ROI_{normalized}^{i,tp} = (ROI^{i,tp} - \min_{i,tp} ROI^{i,tp}) \,/\, (\operatorname{median}_{i,tp} ROI^{i,tp} - \min_{i,tp} ROI^{i.tp})$$

472 This ensured that the minimum value of IEG expression was 0 and the median 1. No blinding of
473 experimental condition was performed in any of the analyses. Statistical tests were used as stated in the
474 figure legends.

475 **Figure 1.** Examples images (**Figures 1B-1D**) are average projections of the recorded channel. IEG
476 expression was normalized as described above (**Figures 1E-1G**). Correlation coefficients (**Figures 1E-1G**)
477 were calculated based on the neuronal population vectors of average activity and IEG expression per
478 measurement timepoint, for each mouse. For the statistical comparison of the correlation coefficients of
479 IEG expression levels with neural activity between the three different groups (4 mice per group), data
480 were bootstrapped 5 times with random replacement and then a t-test was performed on the
481 bootstrapped data.

482 **Figure 2.** To compare changes in neural activity and IEG expression levels between conditions we
483 averaged data from the last two recording sessions of the previous condition and the first two recording
484 sessions of the following condition (**Figures 2B and 2C**). Linear trend analysis (**Figure 2B**) was performed
485 using the MATLAB regress function. To quantify the significance of the linear trend we report the R^2
486 statistic and p-value of the F statistic. Linear fits were performed for each mouse individually using the
487 MATLAB polyfit and polyval functions. Rank order correlation coefficients (**Figures 2D-2F**) were
488 determined based on the population vectors of average IEG expression per measurement timepoint and
489 mouse, and then averaged.

490 **Figure 3.** For plots of event-triggered activity changes $\Delta F/F$ traces were baseline-subtracted by the
491 average $\Delta F/F$ in a window −500 ms to −100 ms preceding the event onset. Z-scores were obtained on a
492 population vector with average stimulus onset values calculated over a response window of 1.5 s. High
493 IEGs neurons were selected as the top 10% of IEG expressing neurons based on average expression level
494 on the first day of condition 3.

495 **Figure 4.** Correlation coefficients (**Figure 4A**) were calculated by correlating each neuron's activity trace
496 with either the running trace or the visual flow trace during open-loop phases. High IEG neurons were
497 selected with the same criteria used for **Figure 3**. Stimulus-triggered fluorescence changes (**Figure 4B**)

498 were mean-subtracted in a window −500 ms to −100 ms preceding the stimulus onset. Responses were
499 quantified in a window of 1.5 s.

500 **Figure S1**. Correlation coefficients of mean or maximum activity with IEG expression were calculated for
501 each mouse (**Figure S1B**). Mice from visual stimulation experiments (**Figure 1**) and sensorimotor learning
502 experiments (**Figures 2-4**) were pooled for this analysis. For mice from the sensorimotor learning
503 experiments the calculation was done using mean or maximum activity of the first recording segment
504 and the last IEG measurement within a session. Shown is the average correlation across all sessions.

505 **Code and data availability.** All imaging and image processing code can be found online at
506 https://sourceforge.net/projects/iris-scanning/ (IRIS, imaging software package) and
507 https://sourceforge.net/p/iris-scanning/calliope/HEAD/tree (Calliope, image processing software
508 package). All the raw data and analysis code used in this study can be downloaded from the following
509 website: http://data.fmi.ch/PublicationSupplementRepo/.

510

511 **ACKNOWLEDGEMENTS**

512 We thank the entire Keller lab for helpful discussion and comments on earlier versions of this
513 manuscript. We thank Daniela Gerosa-Erni for production of the AAV vectors. This work was supported
514 by the Swiss National Science Foundation (GBK), the Novartis Research Foundation (GBK), the Human
515 Frontier Science Program (GBK), and JSPS-Kakenhi and AMED (HO and HB).

516

517 **AUTHOR CONTRIBUTIONS**

518 D.M. and P.Z. performed the experiments, D.M. analyzed the data. H.O. and H.B. made the EGFP-Arc
519 mouse. All authors wrote the manuscript.

520 **REFERENCES**

521 Attinger, A., Wang, B., and Keller, G.B. (2017). Visuomotor Coupling Shapes the Functional Development
522 of Mouse Visual Cortex. Cell *169*, 1291-1302.e14.

523 Bailey, D.J., and Wade, J. (2003). Differential expression of the immediate early genes FOS and ZENK
524 following auditory stimulation in the juvenile male and female zebra finch. Brain Research. Molecular
525 Brain Research *116*, 147–154.

526 Barth, A.L., Gerkin, R.C., and Dean, K.L. (2004). Alteration of Neuronal Firing Properties after In Vivo
527 Experience in a FosGFP Transgenic Mouse. The Journal of Neuroscience *24*, 6466–6475.

528 Bozon, B., Kelly, A., Josselyn, S.A., Silva, A.J., Davis, S., and Laroche, S. (2003). MAPK, CREB and zif268 are
529 all required for the consolidation of recognition memory. Philosophical Transactions of the Royal Society
530 of London. Series B, Biological Sciences *358*, 805–814.

531 Bullitt, E. (1990). Expression of C-fos-like protein as a marker for neuronal activity following noxious
532 stimulation in the rat. The Journal of Comparative Neurology *296*, 517–530.

533 Chang, M.C., Park, J.M., Pelkey, K.A., Grabenstatter, H.L., Xu, D., Linden, D.J., Sutula, T.P., McBain, C.J.,
534 and Worley, P.F. (2010). Narp regulates homeostatic scaling of excitatory synapses on parvalbumin-
535 expressing interneurons. Nat Neurosci *13*, 1090–1097.

536 Chowdhury, S., Shepherd, J.D., Okuno, H., Lyford, G., Petralia, R.S., Plath, N., Kuhl, D., Huganir, R.L., and
537 Worley, P.F. (2006). Arc/Arg3.1 Interacts with the Endocytic Machinery to Regulate AMPA Receptor
538 Trafficking. Neuron *52*, 445–459.

539 Dana, H., Mohar, B., Sun, Y., Narayan, S., Gordus, A., Hasseman, J.P., Tsegaye, G., Holt, G.T., Hu, A.,
540 Walpita, D., et al. (2016). Sensitive red protein calcium indicators for imaging neural activity. ELife *5*.

541 Denny, C.A., Kheirbek, M.A., Alba, E.L., Tanaka, K.F., Brachman, R.A., Laughman, K.B., Tomm, N.K., Turi,
542 G.F., Losonczy, A., and Hen, R. (2014). Hippocampal Memory Traces Are Differentially Modulated by
543 Experience, Time, and Adult Neurogenesis. Neuron *83*, 189–201.

544 Dombeck, D.A., Khabbaz, A.N., Collman, F., Adelman, T.L., and Tank, D.W. (2007). Imaging Large-Scale
545 Neural Activity with Cellular Resolution in Awake, Mobile Mice. Neuron *56*, 43–57.

546 Dombeck, D.A., Harvey, C.D., Tian, L., Looger, L.L., and Tank, D.W. (2010). Functional imaging of
547 hippocampal place cells at cellular resolution during virtual navigation. Nature Neuroscience *13*, 1433–
548 1440.

549 Dudek, S. (2008). Transcriptional Regulation by Neuronal Activity (Boston, MA: Springer US).

550 Farina, F.R., and Commins, S. (2016). Differential expression of immediate early genes Zif268 and c-Fos
551 in the hippocampus and prefrontal cortex following spatial learning and glutamate receptor antagonism.
552 Behavioural Brain Research *307*, 194–198.

553 Fiser, J., Chiu, C., and Weliky, M. (2004). Small modulation of ongoing cortical dynamics by sensory input
554 during natural vision. Nature *431*, 573–578.

555 Fleischmann, A., Hvalby, O., Jensen, V., Strekalova, T., Zacher, C., Layer, L.E., Kvello, A., Reschke, M.,
556 Spanagel, R., Sprengel, R., et al. (2003). Impaired Long-Term Memory and NR2A-Type NMDA Receptor-
557 Dependent Synaptic Plasticity in Mice Lacking c-Fos in the CNS. The Journal of Neuroscience *23*, 9116–
558 9122.

559 Gandolfi, D., Cerri, S., Mapelli, J., Polimeni, M., Tritto, S., Fuzzati-Armentero, M.-T., Bigiani, A., Blandini,
560 F., Mapelli, L., and D'Angelo, E. (2017). Activation of the CREB/c-FosPathway during Long-Term Synaptic
561 Plasticity in the Cerebellum Granular Layer. Frontiers in Cellular Neuroscience *11*, 184.

562 Gao, M., Sossa, K., Song, L., Errington, L., Cummings, L., Hwang, H., Kuhl, D., Worley, P., and Lee, H.-K.
563 (2010). A Specific Requirement of Arc/Arg3.1 for Visual Experience-Induced Homeostatic Synaptic
564 Plasticity in Mouse Primary Visual Cortex. The Journal of Neuroscience *30*, 7168–7178.

565 Garner, A.R., Rowland, D.C., Hwang, S.Y., Baumgaertel, K., Roth, B.L., Kentros, C., and Mayford, M.
566 (2012). Generation of a Synthetic Memory Trace. Science (New York, N.Y.) *335*, 1513–1516.

567 Greenberg, M.E., and Ziff, E.B. (1984). Stimulation of 3T3 cells induces transcription of the c-fos proto-
568 oncogene. Nature *311*, 433–438.

569 Gu, Y., Huang, S., Chang, M.C., Worley, P., Kirkwood, A., and Quinlan, E.M. (2013). Obligatory Role for
570 the Immediate Early Gene NARP in Critical Period Plasticity. Neuron *79*, 335–346.

571 Guzowski, J.F. (2002). Insights into immediate-early gene function in hippocampal memory consolidation
572 using antisense oligonucleotide and fluorescent imaging approaches. Hippocampus *12*, 86–104.

573 Guzowski, J.F., and McGaugh, J.L. (1997). Antisense oligodeoxynucleotide-mediated disruption of
574 hippocampal cAMP response element binding protein levels impairs consolidation of memory for water
575 maze training. Proceedings of the National Academy of Sciences of the United States of America *94*,
576 2693–2698.

577 Guzowski, J.F., McNaughton, B.L., Barnes, C.A., and Worley, P.F. (1999). Environment-specific expression
578 of the immediate-early gene Arc in hippocampal neuronal ensembles. Nature Neuroscience *2*, 1120–
579 1124.

580 Guzowski, J.F., Lyford, G.L., Stevenson, G.D., Houston, F.P., McGaugh, J.L., Worley, P.F., and Barnes, C. a
581 (2000). Inhibition of activity-dependent arc protein expression in the rat hippocampus impairs the
582 maintenance of long-term potentiation and the consolidation of long-term memory. The Journal of
583 Neuroscience : The Official Journal of the Society for Neuroscience *20*, 3993–4001.

584 Guzowski, J.F., Miyashita, T., Chawla, M.K., Sanderson, J., Maes, L.I., Houston, F.P., Lipa, P., McNaughton,
585 B.L., Worley, P.F., and Barnes, C.A. (2006). Recent behavioral history modifies coupling between cell
586 activity and Arc gene transcription in hippocampal CA1 neurons. Proceedings of the National Academy
587 of Sciences of the United States of America *103*, 1077–1082.

588 Hengen, K.B., Torrado Pacheco, A., McGregor, J.N., Van Hooser, S.D., and Turrigiano, G.G. (2016).
589 Neuronal Firing Rate Homeostasis Is Inhibited by Sleep and Promoted by Wake. Cell *165*, 180–191.

590 Holtmaat, A., and Caroni, P. (2016). Functional and structural underpinnings of neuronal assembly
591 formation in learning. Nature Neuroscience *19*, 1553–1562.

592 Jarvis, E.D., Ribeiro, S., Da Silva, M.L., Ventura, D., Vielliard, J., and Mello, C. V. (2000). Behaviourally
593 driven gene expression reveals song nuclei in hummingbird brain. Nature *406*, 628–632.

594 Jenks, K.R., Kim, T., Pastuzyn, E.D., Okuno, H., Taibi, A. V, Bito, H., Bear, M.F., and Shepherd, J.D. (2017).
595 Arc restores juvenile plasticity in adult mouse visual cortex. Proceedings of the National Academy of
596 Sciences *114*, 9182–9187.

597 Jones, M.W., Errington, M.L., French, P.J., Fine, A., Bliss, T.V.P., Garel, S., Charnay, P., Bozon, B., Laroche,
598 S., and Davis, S. (2001). A requirement for the immediate early gene Zif268 in the expression of late LTP
599 and long-term memories. Nature Neuroscience *4*, 289–296.

600 Jordan, R., and Keller, G.B. (2020). Opposing Influence of Top-down and Bottom-up Input on Excitatory
601 Layer 2/3 Neurons in Mouse Primary Visual Cortex. Neuron *108*, 1194-1206.e5.

602 Josselyn, S.A., Köhler, S., and Frankland, P.W. (2015). Finding the engram. Nature Reviews Neuroscience
603 *16*, 521–534.

604 Kaminska, B., Kaczmarek, L., and Chaudhuri, A. (1996). Visual Stimulation Regulates the Expression of
605 Transcription Factors and Modulates the Composition of AP-1 in Visual Cortexa. Journal of
606 Neuroscience *16*, 3968–3978.

607 Kaplan, I. V, Guo, Y., and Mower, G.D. (1996). Immediate early gene expression in cat visual cortex
608 during and after the critical period: differences between EGR-1 and Fos proteins. Brain Research.
609 Molecular Brain Research *36*, 12–22.

610 Kawashima, T., Kitamura, K., Suzuki, K., Nonaka, M., Kamijo, S., Takemoto-Kimura, S., Kano, M., Okuno,
611 H., Ohki, K., and Bito, H. (2013). Functional labeling of neurons and their projections using the synthetic
612 activity–dependent promoter E-SARE. Nature Methods *10*, 889–895.

613 Keck, T., Keller, G.B., Jacobsen, R.I., Eysel, U.T., Bonhoeffer, T., and Hübener, M. (2013). Synaptic scaling
614 and homeostatic plasticity in the mouse visual cortex in vivo. Neuron *80*.

615 Keller, G.B., and Mrsic-Flogel, T.D. (2018). Predictive Processing: A Canonical Cortical Computation.
616 Neuron *100*, 424–435.

617 Keller, G.B., Bonhoeffer, T., and Hübener, M. (2012). Sensorimotor mismatch signals in primary visual
618 cortex of the behaving mouse. Neuron *74*, 809–815.

619 Knapska, E., and Kaczmarek, L. (2004). A gene for neuronal plasticity in the mammalian brain:
620 Zif268/Egr-1/NGFI-A/Krox-24/TIS8/ZENK? Progress in Neurobiology *74*, 183–211.

621 Leinweber, M., Zmarz, P., Buchmann, P., Argast, P., Hübener, M., Bonhoeffer, T., and Keller, G.B. (2014).
622 Two-photon calcium imaging in mice navigating a virtual reality environment. Journal of Visualized
623 Experiments : JoVE e50885.

624 Leinweber, M., Ward, D.R., Sobczak, J.M., Attinger, A., and Keller, G.B. (2017). A Sensorimotor Circuit in
625 Mouse Cortex for Visual Flow Predictions. Neuron *95*, 1420-1432.e5.

Liu, X., Ramirez, S., Pang, P.T., Puryear, C.B., Govindarajan, A., Deisseroth, K., and Tonegawa, S. (2012). Optogenetic stimulation of a hippocampal engram activates fear memory recall. Nature *484*, 381–385.

Mahringer, D., Petersen, A., Fiser, A., Okuno, H., Bito, H., Perrier, J.-F., and Keller, G. (2019). Expression of c-Fos and Arc in hippocampal region CA1 marks neurons that exhibit learning-related activity changes. BioRxiv 644526.

Makino, H., and Komiyama, T. (2015). Learning enhances the relative impact of top-down processing in the visual cortex. Nature Neuroscience *18*, 1116–1122.

Mataga, N., Fujishima, S., Condie, B.G., and Hensch, T.K. (2001). Experience-Dependent Plasticity of Mouse Visual Cortex in the Absence of the Neuronal Activity-Dependent Markeregr1/zif268 . The Journal of Neuroscience *21*, 9724–9732.

McCurry, C.L., Shepherd, J.D., Tropea, D., Wang, K.H., Bear, M.F., and Sur, M. (2010). Loss of Arc renders the visual cortex impervious to the effects of sensory experience or deprivation. Nature Neuroscience *13*, 450–457.

Messaoudi, E., Kanhema, T., Soulé, J., Tiron, A., Dagyte, G., da Silva, B., and Bramham, C.R. (2007). Sustained Arc/Arg3.1 synthesis controls long-term potentiation consolidation through regulation of local actin polymerization in the dentate gyrus in vivo. The Journal of Neuroscience : The Official Journal of the Society for Neuroscience *27*, 10445–10455.

Minatohara, K., Akiyoshi, M., and Okuno, H. (2015). Role of Immediate-Early Genes in Synaptic Plasticity and Neuronal Ensembles Underlying the Memory Trace. Frontiers in Molecular Neuroscience *8*, 78.

Mo, J., Kim, C.-H., Lee, D., Sun, W., Lee, H.W., and Kim, H. (2015). Early growth response 1 (Egr-1) directly regulates GABA receptor α2, α4, and θ subunits in the hippocampus. Journal of Neurochemistry *133*, 489–500.

Morgan, J.I., Cohen, D.R., Hempstead, J.L., and Curran, T. (1987). Mapping patterns of c-fos expression in the central nervous system after seizure. Science *237*, 192–197.

Okuno, H., Akashi, K., Ishii, Y., Yagishita-Kyo, N., Suzuki, K., Nonaka, M., Kawashima, T., Fujii, H., Takemoto-Kimura, S., Abe, M., et al. (2012). Inverse synaptic tagging of inactive synapses via dynamic interaction of Arc/Arg3.1 with CaMKIIβ. Cell *149*, 886–898.

Paxinos, G., and Franklin, K.B.J. (2013). Paxinos and Franklin's the mouse brain in stereotaxic coordinates (Academic Press).

Petreanu, L., Mao, T., Sternson, S.M., and Svoboda, K. (2009). The subcellular organization of neocortical excitatory connections. Nature *457*, 1142–1145.

Ploski, J.E., Pierre, V.J., Smucny, J., Park, K., Monsey, M.S., Overeem, K.A., and Schafe, G.E. (2008). The activity-regulated cytoskeletal-associated protein (Arc/Arg3.1) is required for memory consolidation of pavlovian fear conditioning in the lateral amygdala. Journal of Neuroscience *28*, 12383–12395.

Ramirez, S., Liu, X., Lin, P.-A., Suh, J., Pignatelli, M., Redondo, R.L., Ryan, T.J., and Tonegawa, S. (2013). Creating a false memory in the hippocampus. Science (New York, N.Y.) *341*, 387–391.

662 Ramírez-Amaya, V., Vazdarjanova, A., Mikhael, D., Rosi, S., Worley, P.F., and Barnes, C.A. (2005). Spatial
663 Exploration-Induced Arc mRNA and Protein Expression: Evidence for Selective, Network-Specific
664 Reactivation. The Journal of Neuroscience *25*, 1761–1768.

665 Reijmers, L.G., Perkins, B.L., Matsuo, N., and Mayford, M. (2007). Localization of a stable neural
666 correlate of associative memory. Science (New York, N.Y.) *317*, 1230–1233.

667 Rial Verde, E.M., Lee-Osbourne, J., Worley, P.F., Malinow, R., and Cline, H.T. (2006). Increased
668 Expression of the Immediate-Early Gene Arc/Arg3.1 Reduces AMPA Receptor-Mediated Synaptic
669 Transmission. Neuron *52*, 461–474.

670 Rosen, K.M., McCormack, M.A., Villa-Komaroff, L., and Mower, G.D. (1992). Brief visual experience
671 induces immediate early gene expression in the cat visual cortex. Proceedings of the National Academy
672 of Sciences of the United States of America *89*, 5437–5441.

673 Saleem, A.B., Ayaz, A., Jeffery, K.J., Harris, K.D., and Carandini, M. (2013). Integration of visual motion
674 and locomotion in mouse visual cortex. Nature Neuroscience *16*, 1864–1869.

675 Shepherd, J.D., and Bear, M.F. (2011). New views of Arc, a master regulator of synaptic plasticity. Nature
676 Neuroscience *14*, 279–284.

677 Shepherd, J.D., Rumbaugh, G., Wu, J., Chowdhury, S., Plath, N., Kuhl, D., Huganir, R.L., and Worley, P.F.
678 (2006). Arc/Arg3.1 Mediates Homeostatic Synaptic Scaling of AMPA Receptors. Neuron *52*, 475–484.

679 Steward, O., Matsudaira Yee, K., Farris, S., Pirbhoy, P.S., Worley, P., Okamura, K., Okuno, H., and Bito, H.
680 (2017). Delayed Degradation and Impaired Dendritic Delivery of Intron-Lacking EGFP-Arc/Arg3.1 mRNA
681 in EGFP-Arc Transgenic Mice. Frontiers in Molecular Neuroscience *10*, 435.

682 Tagawa, Y., Kanold, P.O., Majdan, M., and Shatz, C.J. (2005). Multiple periods of functional ocular
683 dominance plasticity in mouse visual cortex. Nature Neuroscience *8*, 380–388.

684 Torrado Pacheco, A., Tilden, E.I., Grutzner, S.M., Lane, B.J., Wu, Y., Hengen, K.B., Gjorgjieva, J., and
685 Turrigiano, G.G. (2019). Rapid and active stabilization of visual cortical firing rates across light-dark
686 transitions. Proc Natl Acad Sci U S A *116*, 18068–18077.

687 Tzingounis, A. V., and Nicoll, R.A. (2006). Arc/Arg3.1: Linking Gene Expression to Synaptic Plasticity and
688 Memory. Neuron *52*, 403–407.

689 Vazdarjanova, A., Ramirez-Amaya, V., Insel, N., Plummer, T.K., Rosi, S., Chowdhury, S., Mikhael, D.,
690 Worley, P.F., Guzowski, J.F., and Barnes, C.A. (2006). Spatial exploration induces ARC, a plasticity-related
691 immediate-early gene, only in calcium/calmodulin-dependent protein kinase II-positive principal
692 excitatory and inhibitory neurons of the rat forebrain. The Journal of Comparative Neurology *498*, 317–
693 329.

694 Veyrac, A., Besnard, A., Caboche, J., Davis, S., and Laroche, S. (2014). The Transcription Factor
695 Zif268/Egr1, Brain Plasticity, and Memory. Progress in Molecular Biology and Translational Science *122*,
696 89–129.

697 Wang, G., Xie, H., Hu, Y., Chen, Q., Liu, C., Liu, K., Yan, Y., and Guan, J.-S. (2021). Egr1-EGFP transgenic
698 mouse allows in vivo recording of Egr1 expression and neural activity. J Neurosci Methods *363*, 109350.

699 Wang, K.H., Majewska, A., Schummers, J., Farley, B., Hu, C., Sur, M., and Tonegawa, S. (2006). In vivo
700 two-photon imaging reveals a role of arc in enhancing orientation specificity in visual cortex. Cell *126*,
701 389–402.

702 Waung, M.W., Pfeiffer, B.E., Nosyreva, E.D., Ronesi, J.A., and Huber, K.M. (2008). Rapid Translation of
703 Arc/Arg3.1 Selectively Mediates mGluR-Dependent LTD through Persistent Increases in AMPAR
704 Endocytosis Rate. Neuron *59*, 84–97.

705 Weng, F.-J., Garcia, R.I., Lutzu, S., Alviña, K., Zhang, Y., Dushko, M., Ku, T., Zemoura, K., Rich, D., Garcia-
706 Dominguez, D., et al. (2018). Npas4 Is a Critical Regulator of Learning-Induced Plasticity at Mossy Fiber-
707 CA3 Synapses during Contextual Memory Formation. Neuron.

708 Widmer, F.C., and Keller, G.B. (2021). Developmental plasticity in visual cortex is necessary for normal
709 visuomotor integration and visuomotor skill learning. BioRxiv 2021.06.20.449148.

710 Xie, H., Liu, Y., Zhu, Y., Ding, X., Yang, Y., and Guan, J.-S. (2014). In vivo imaging of immediate early gene
711 expression reveals layer-specific memory traces in the mammalian brain. Proceedings of the National
712 Academy of Sciences *111*, 2788–2793.

713 Yamada, Y., Hada, Y., Imamura, K., Mataga, N., Watanabe, Y., and Yamamoto, M. (1999). Differential
714 expression of immediate-early genes, c-fos and zif268, in the visual cortex of young rats: effects of a
715 noradrenergic neurotoxin on their expression. Neuroscience *92*, 473–484.

716 Yap, E.-L., and Greenberg, M.E. (2018). Activity-Regulated Transcription: Bridging the Gap between
717 Neural Activity and Behavior. Neuron *100*, 330–348.

718 Yasoshima, Y., Sako, N., Senba, E., and Yamamoto, T. (2006). Acute suppression, but not chronic genetic
719 deficiency, of c-fos gene expression impairs long-term memory in aversive taste learning. Proceedings of
720 the National Academy of Sciences of the United States of America *103*, 7106–7111.

721 Yassin, L., Benedetti, B.L., Jouhanneau, J.S., Wen, J.A., Poulet, J.F.A., and Barth, A.L. (2010). An
722 Embedded Subnetwork of Highly Active Neurons in the Neocortex. Neuron *68*, 1043–1050.

723 Zmarz, P., and Keller, G.B. (2016). Mismatch Receptive Fields in Mouse Visual Cortex. Neuron *92*, 766–
724 772.

725